SCIENCE CHINA
Technological Sciences

• Article •

May 2016 Vol.59 No.5: 699–708
doi: 10.1007/s11431-016-6042-1

# Sound absorption coefficient optimization of gradient sintered metal fiber felts

MENG Han[1,2], REN ShuWei[1,2], XIN FengXian[1,2*] & LU TianJian[1,2*]

[1] *MOE Key Laboratory for Multifunctional Materials and Structures, Xi'an Jiaotong University, Xi'an 710049, China;*
[2] *State Key Laboratory for Strength and Vibration of Mechanical Structures, Xi'an Jiaotong University, Xi'an 710049, China*

Received January 15, 2016; accepted March 14, 2016; published online April 18, 2016

An optimization method for sound absorption of gradient (multi-layered) sintered metal fiber felts is presented. The theoretical model based on dynamic flow resistivity is selected to calculate the sound absorption coefficient of the sintered metal fiber felts since it only requires three key morphological parameters: fiber diameter, porosity and layer thickness. The model predictions agree well with experimental measurements. Objective functions and constraint conditions are then set up to optimize separately the distribution of porosity, fiber diameter, and simultaneous porosity and fiber diameter in the metal fiber. The optimization problem for either a sole frequency or a pre-specified frequency range is solved using a genetic algorithm method. Acoustic performance comparison between optimized and non-optimized metal fibers is presented to confirm the effectiveness of the optimization method. Gradient sintered metal fiber felts hold great potential for noise control applications particularly when stringent restriction is placed on the total volume and/or weight of sound absorbing material allowed to use.

**sound absorption, optimization, sintered metal fiber felts**

**Citation:** Meng H, Ren S W, Xin F X, et al. Sound absorption coefficient optimization of gradient sintered metal fiber felts. Sci China Tech Sci, 2016, 59: 699–708, doi: 10.1007/s11431-016-6042-1

## 1 Introduction

Lightweight sintered metal fiber felts are typically fabricated using metal fibers (stainless steel, FeCrAl, etc.) with micro-size diameters. The metal fibers are firstly cut into 10–50 mm long pieces, then arranged to form 2D (two-dimensional) random overlapping metal fiber felt (e.g., in a purposely-designed mould with external compressive force applied), and finally sintered at high temperature, followed by naturally cooling down in the furnace. A gradient sintered metal fiber felt may be fabricated by sintering several metal fiber felt layers having different morphological parameters that are stacked on top of each other. In general, the properties of the gradient metal fiber felts fabricated using this way vary only along its thickness direction.

Compared with conventional fibrous materials (polyester, wood, etc.), sintered metal fiber felts exhibit many advantages: simple manufacturing process, high porosity (e.g., 80% or higher) and sound absorption ability, good mechanical and thermal (e.g., conductive and convective heat transfer) properties, and high temperature resistance, etc. As a result, sintered metal fibers are particularly applicable for noise control in extreme circumstances, such as acoustical liner of turbofan engine inlet [1–4]. However, the sound absorption coefficient of a sintered metal fiber felt varies significantly with frequency and, in particular, its performance at low frequencies is not as good as that at high frequencies. Our previous study [5] demonstrated that the sound absorption coefficient is determined by the distribution of key morphological parameters inside the metal fiber,

*Corresponding authors (email: fengxian.xin@gmail.com; tjlu@mail.xjtu.edu.cn)

e.g., fiber diameter and porosity. To improve the acoustic performance of metal fiber at low frequencies, the present study aims to present a method to optimize the distribution of these parameters.

Theoretical models for sound propagation in sintered metal fiber felts are needed to optimize the sound absorption coefficient. Thus far, a multitude of such models have been developed on the basis of empirical modeling. For instance, Delany and Bazley [6] presented empirical functions between sound absorption coefficient and static flow resistance of fibrous materials. Subsequently, Miki [7] and Komatsu [8] modified the empirical model of Delany and Bazley in order to obtain more accurate predictions of sound absorption coefficient. Also based on the static flow resistivity, Allard and Champoux [9] proposed a new empirical model for sound propagation in rigid frame fibrous materials and showed that, at low frequencies, the model was more accurate than the Delany-Bazley model. Apart from the above empirical models, several phenomenological models for fibrous materials have been developed using key morphological parameters. For instance, Attenborough [10], Lambert and Tesar [11], Allard and Atalla [12], and Zhang and Chen [13] set up theoretical models based on parameters related to the shape factor of the pores in fiber materials (e.g., porosity, flow resistivity, tortuosity, viscous and thermal characteristic length). Due to the complexity of the microstructures of fiber materials, these parameters involved in the empirical and phenomenological models are difficult to be quantified. Often, these parameters were determined by experimental measurements [14–18]. Therefore, it is difficult to optimize the sound absorption coefficient by directly adopting these two kinds of models with non- controllable parameters. Whereas, by assuming the fibers are distributed in periodic hexagonal patterns, Liu and Chen et al. [19,20] favorably optimized the sound absorption coefficient of porous fibrous materials by using a phenomenological model.

There also exist theoretical models for estimating the acoustical properties of rigid frame fibrous materials using key controllable parameters, such as the ones developed by Tarnow [21,22], Dupère et al. [23,24], Sun et al. [1] and Kirby and Cumming [25]. These authors calculated the flow resistivity, compressibility and sound absorption coefficient by using the porosity and fiber diameter as the fundamental parameters. Especially, the theoretical model developed by Meng et al. [5] to calculate the sound absorption coefficient of gradient sintered metal fiber felts is deemed suitable for acoustic optimization. In the present study, the theoretical model of Meng et al. [5] is introduced and validated by comparison with experimentally measured sound absorption coefficients of sintered metal fiber samples. Based upon the model, the objective functions and constraint conditions for sound absorption coefficient optimization are presented. The optimized porosity and fiber diameter distributions are subsequently obtained using a genetic algorithm method, both for a sole frequency and a pre-specified frequency range. Finally, performance comparison between optimized and non-optimized metal fiber felts is presented to confirm the effectiveness of the optimization method.

## 2 Theoretical model

The sound absorption coefficient of a sintered metal fiber layer as shown in Figure 1 is calculated using the dynamic flow resistivity based model previously developed by the authors [5]. For sound normally incident on the surface of the metal fiber felt, the sound wave is vertical to all the fibers. As a result, the dynamic flow resistivity of the metal fiber felt may be approximately evaluated by examining an array of randomly distributed parallel fibers [5] having equivalent porosity as that of the randomly distributed fibers, as shown schematically in Figure 2(a). Contribution of the sintered points to flow resistance is ignored as they occupy much less surface area in comparison with the fibers. It is assumed that the metal fibers are cylindrical and have sufficiently large length to diameter ratios to be considered as infinitely long. Further, for the linear acoustic problem considered in the present study, they are taken as rigid.

For fluid flowing perpendicularly pass the cylindrical fibers (Figure 2(b)), the dynamic flow resistivity of the fibers may be calculated using a self-consistent Brinkman approach, as [5,22]

$$R_{\perp} = -j\omega\rho_0 + \frac{2\pi\eta k'_{\perp} a}{b^2}\left(-k'_{\perp} a + \frac{2H_1^1(k'_{\perp} a)}{H_0^1(k'_{\perp} a)}\right), \tag{1}$$

where $j$ is the unit value of the complex number, $\omega$ is the angular frequency, $\rho_0$ and $\eta$ are the density and dynamic

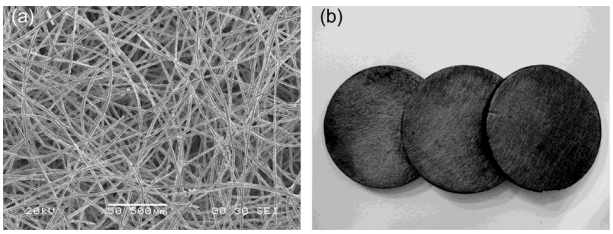


**Figure 1** Sintered metal fiber felt: (a) Planar view and (b) samples for impedance tube test.

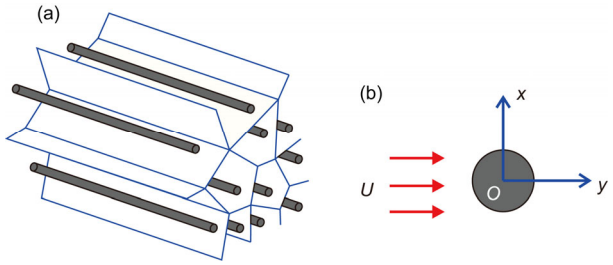


**Figure 2** (Color online) (a) Array of randomly distributed parallel fibers and (b) fluid flow pass one fiber.

viscosity of the fluid around the fibers, $a$ is the radius of the fibers, $b^2=\pi a^2/(1-\Omega)$ is the averaged area of the Voronoi-type irregular polygons around the fibers (Figure 2(a)), $\Omega$ is the porosity of the metal fiber felt, $H_i^1(\cdot)$ is the $i$th order Hankel function of the first kind, and

$$k'_\perp=\sqrt{\frac{-R_\perp}{\eta}}. \tag{2}$$

The dynamic flow resistivity is obtained by solving eqs. (1) and (2) iteratively [5].

Once the dynamic resistivity is determined, the propagation constant and characteristic impedance of the sintered metal fiber felt can be calculated using the empirical formulas of Komatsu [8], as follows. The propagation constant $\Gamma$ is

$$\begin{aligned}\Gamma=&0.0069\frac{\omega}{c_0}\left(2-\log\frac{f}{R_\perp}\right)^{4.1}\\&+j\frac{\omega}{c_0}\left[1+0.0004\left(2-\log\frac{f}{R_\perp}\right)^{6.2}\right],\end{aligned} \tag{3}$$

where $c_0$ is sound speed in fluid around the fibers and $f$ is the frequency. The characteristic impedance $Z$ is

$$\begin{aligned}Z=&\rho_0c_0\left[1+0.00027\left(2-\log\frac{f}{R_\perp}\right)^{6.2}\right]\\&-j\rho_0c_0\left[0.0047\left(2-\log\frac{f}{R_\perp}\right)^{4.1}\right].\end{aligned} \tag{4}$$

For a uniform metal fiber sample of thickness $h$ backed by an impervious rigid wall, the surface impedance is calculated by the propagation constant and characteristic impedance, as

$$Z_s(f)=Z(f)\coth\left[\Gamma(f)h\right]. \tag{5}$$

Correspondingly, the sound absorption coefficient of the sample is obtained as

$$\alpha=1-\left|\frac{Z_s-\rho_0c_0}{Z_s+\rho_0c_0}\right|^2. \tag{6}$$

With reference to Figure 3, for a gradient sample composed of $n$ layers of different sintered metal fiber felts, also backed by a rigid wall, the recursion formula for surface impedance is

$$Z_s(x_n)=Z_{n-1}\frac{Z_s(x_{n-1})\coth(\Gamma_{n-1}d_{n-1})+Z_{n-1}}{Z_s(x_{n-1})+Z_{n-1}\coth(\Gamma_{n-1}d_{n-1})}, \tag{7}$$

where $Z_{n-1}$, $d_{n-1}$ and $\Gamma_{n-1}$ are the characteristic impedance, thickness and the propagation constant of the $(n-1)$th layer, respectively. Substitution of eq. (7) into eq. (6), the sound absorption coefficient of the gradient metal fiber felt can be calculated.

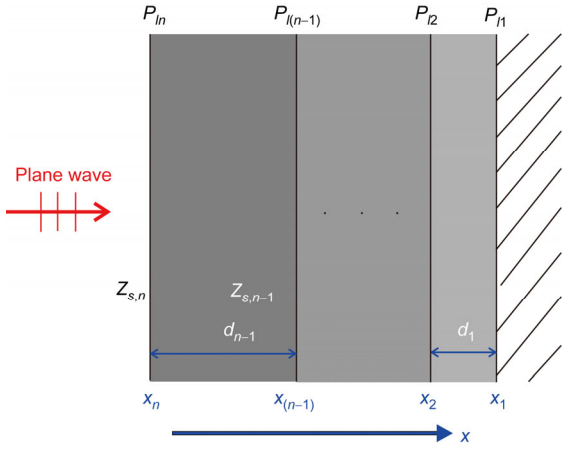


**Figure 3** (Color online) Schematic of sound incident on gradient (multilayer) sintered metal fiber felt.

Even though the model based upon dynamic flow resistivity has been validated by Meng et al. [5], we measured the sound absorption coefficients of 4 sintered metal fiber samples using the impedance tube method and compared the experimental results with the model predictions in Figure 4. The physical parameters of the tested samples are listed in Table 1. Overall, the sound absorption coefficients predicted by the dynamic flow resistivity model fit well with the test data. The model is then applied in the next section to perform systematic optimization studies on sintered metal fiber felts.

## 3 Optimization

Based on the dynamic flow resistivity based model described in Section 2, we present a sound absorption coefficient optimization procedure for gradient sintered metal fiber felts. It can be seen from the model that the sound absorption coefficient of a sintered metal fiber sample is determined by its fiber diameter and porosity. Thus, before carrying out the optimization, the influence of fiber diameter and porosity on the sound absorption performance of uniform sintered metal fiber felts is discussed first to provide reference for subsequent optimization.

The model predictions presented in Figure 5 demonstrate that, for a uniform sintered metal fiber felt, its sound absorption capability is significantly affected by both porosity and fiber diameter. As the porosity is increased while the fiber diameter is fixed, the sound absorption coefficient decreases at relatively low frequencies but increases at higher frequencies (Figure 5(a)). A similar variation trend is observed when the fiber diameter is increased while the

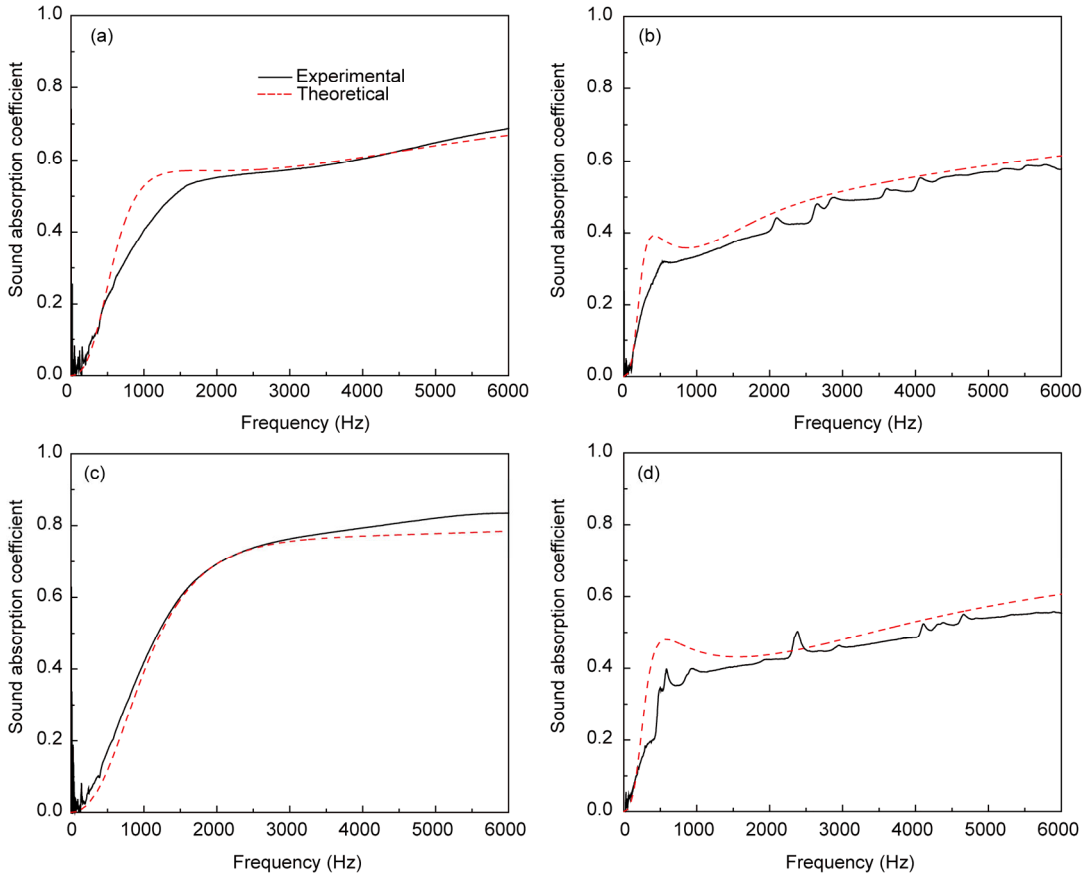


**Figure 4** (Color online) Sound absorption coefficient of sintered metal fiber samples: Comparison between model predictions and experimental measurements. (a) Sample a#; (b) sample b#; (c) sample c#; (d) sample d#. Sample d# is gradient, while samples a#, b# and c# are uniform (Table 1).

**Table 1** Physical parameters of sintered metal fiber samples

| Sample number | Layer | Fiber diameter (μm) | Porosity (%) | Thickness of layer (mm) |
|---|---|---|---|---|
| a# | Single layer | 8 | 90 | 10 |
| b# | Single layer | 6.5 | 90 | 15 |
| c# | Single layer | 12 | 90 | 10 |
| | 1st | 6.5 | 90 | 5 |
| d# | 2nd | 12 | 90 | 5 |
| | 3rd | 20 | 90 | 5 |

porosity is fixed (Figure 5(b)). Increasing the fiber diameter (with porosity fixed) shifts the sound absorption coefficient curve to higher frequencies: sound absorption decreases with increasing fiber diameter at low frequencies but increases when the frequency becomes sufficiently high. The physical mechanisms underlying these changes are mainly linked to viscous and thermal forces that are in play during the process of sound energy dissipation in metal fiber felts [5].

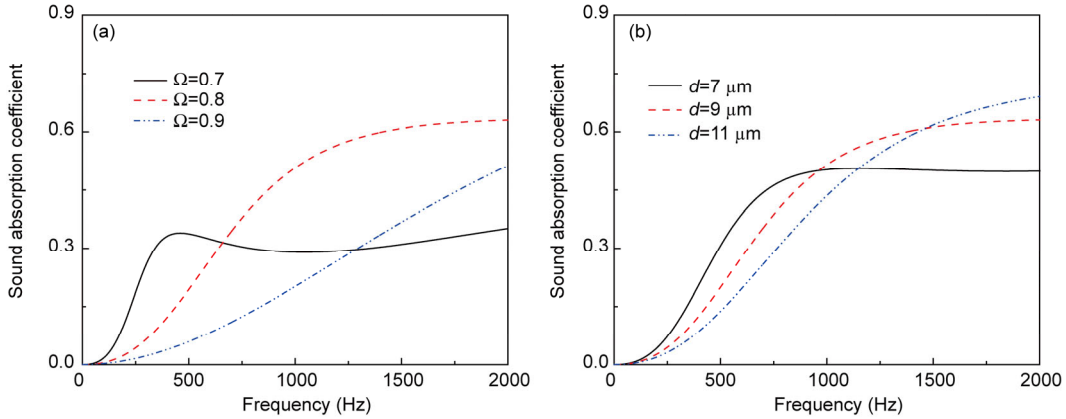


**Figure 5** (Color online) (a) Influence of porosity on sound absorption coefficient of uniform sintered metal fiber (sample thickness 10 mm and fiber diameter 20 μm). (b) Influence of fiber diameter on sound absorption coefficient of uniform sintered metal fiber (sample thickness 10 mm and porosity 0.9).

In certain practical applications where weight and/or volume are of critical concern, a limit is usually placed upon the amount (e.g., thickness of layer) of fibrous sound absorbing material that is allowed to use. A good example is the vibration damping and acoustic shielding of key electronic devices in aerospace technologies. Therefore, an optimization method of sound absorption is proposed in the following section for gradient sintered metal fiber felt (Figure 3) under the restriction that its total thickness is fixed. Relevant objective functions and constraints are proposed for porosity optimization, fiber diameter optimization, and simultaneous porosity and fiber diameter optimization.

### 3.1 Optimization of porosity distribution

#### *3.1.1 Optimization at a sole frequency*

To optimize the distribution of porosity in a multi-layered sintered metal fiber felt (Figure 3) at a sole frequency, the objective function for sound absorption coefficient α may be written as

$$\max\ f\left(\Omega_1,h_1,\cdots,\Omega_n,h_n\right)=\alpha\left(\Omega_1,h_1,\cdots,\Omega_n,h_n\right), \tag{8}$$

where $\alpha\left(\Omega_1,h_1,\cdots,\Omega_n,h_n\right)$ is the sound absorption coefficient of the metal fiber multilayer, $\Omega_i$ and $h_i$ ($i=1,2,\cdots,n$) represent the porosity and thickness of the *i*th layer, and *n* is the total number of layers. The diameter of all fibers in the metal fiber is fixed.

The porosity should be bigger than zero but smaller than unity, while the thickness of each layer should be bigger than the diameter of fibers in the layer. For the case that the volume of the material is fixed, the total thickness of the sample is pre-specified. Therefore, the constraints of the objective function are

$$\begin{aligned} s.t.\quad & 0<\Omega_i<1,\\ & d<h_i<h_p,\\ & \sum_{i=1}^{n}h_i=h_p,\\ & i=1,2,\cdots,n, \end{aligned} \tag{9}$$

where $h_p$ is the expected sample thickness.

#### *3.1.2 Optimization within a frequency range*

For porosity optimization within a pre-specified frequency range, the objective function should be the sum of sound absorption coefficients in the pre-specified frequency range, as

$$\max\ f\left(\Omega_1,h_1,\cdots,\Omega_n,h_n\right)=\int_{f_l}^{f_u}\alpha\left(\Omega_1,h_1,\cdots,\Omega_n,h_n\right)\mathrm{d}f, \tag{10}$$

where $f_l$ and $f_u$ are the lower and upper bound of the pre-specified frequency range. the constraints are the same as those detailed in eq. (9) for the case of sole-frequency optimization.

### 3.2 Optimization of fiber diameter distribution

#### *3.2.1 Optimization at a sole frequency*

To optimize the distribution of fiber diameter at a single frequency, the objective function may be written as

$$\max\ f\left(d_1,h_1,\cdots,d_n,h_n\right)=\alpha\left(d_1,h_1,\cdots,d_n,h_n\right), \tag{11}$$

where $\alpha\left(d_1,h_1,\cdots,d_n,h_n\right)$ is the sound absorption coefficient and $d_i$ is the diameter of fibers in the *i*th layer. In this case, the porosity of the metal fiber multilayer is fixed.

Although in theory the fiber diameter may vary from infinitely small to infinitely large, in practice there is a lower bound of fiber diameter as set by the particular type of manufacturing technology employed to fabricate the metal fiber. In the present study, the smallest fiber diameter is set to be 6.5 μm. The constraints of the objective function are thence:

$$\begin{aligned} s.t.\quad & d_i\ge 6.5\times10^{-6},\\ & d_i<h_i<h_p,\\ & \sum_{i=1}^{n}h_i=h_p,\\ & i=1,2,\cdots,n. \end{aligned} \tag{12}$$

#### *3.2.2 Optimization within a frequency range*

For fiber diameter optimization within a pre-specified frequency range, the objective function is

$$\max\ f\left(d_1,h_1,\cdots,d_n,h_n\right)=\int_{f_l}^{f_u}\alpha\left(d_1,h_1,\cdots,d_n,h_n\right)\mathrm{d}f, \tag{13}$$

subjected to the same constraints of (12) for the case of sole-frequency optimization.

### 3.3 Optimization of simultaneous porosity and fiber diameter distribution

#### *3.3.1 Optimization at a sole frequency*

To optimize simultaneously the distribution of fiber diameter and porosity at a single frequency, the objective function for sound absorption coefficient may be written as

$$\begin{aligned} &\max\ f\left(d_1,\Omega_1,h_1,\cdots,d_n,\Omega_n,h_n\right)\\ &=\alpha\left(d_1,\Omega_1,h_1,\cdots,d_n,\Omega_n,h_n\right), \end{aligned} \tag{14}$$

where $d_i$, $\Omega_i$ and $h_i$ ($i=1,2,\cdots,n$) represent fiber diameter, porosity and thickness of the *i*th layer of the metal fiber sample.

Constraints for porosity, fiber diameter and layer thickness are identical to those given in (9) and (12):

$$\begin{aligned} s.t.\quad & d_i \geq 6.5\times10^{-6}, \\ & 0<\Omega_i<1, \\ & d_i<h_i<h_p, \\ & \sum_{i=1}^{n} h_i = h_p, \\ & i=1,2,\cdots,n. \end{aligned} \tag{15}$$

### 3.3.2 *Optimization within a frequency range*

For optimization within a pre-specified frequency range, the objective function is

$$\begin{aligned} &\max\ f\left(d_1,\Omega_1,h_1,\cdots,d_n,\Omega_n,h_n\right) \\ &=\int_{f_l}^{f_u}\alpha\left(d_1,\Omega_1,h_1,\cdots,d_n,\Omega_n,h_n\right)\mathrm{d}f, \end{aligned} \tag{16}$$

and the constraints are identical to those of (15).

Since the objective functions presented above are all complex multimodal non-differentiable functions, a genetic algorithm optimization strategy is applied to solve the optimization problem [26].

## 4 Numerical results and discussion

On the basis of the theoretical model presented in Section 2 and the optimization method detailed in Section 3, selected numerical results are presented in this section to demonstrate the feasibility of the proposed optimization approach.

### 4.1 Optimized porosity distribution

To optimize the porosity distribution, the multilayer metal fiber sample as shown in Figure 3 has a fixed total thickness of 10 mm, which is relatively small, and a fixed fiber diameter of 20 μm, which is typical for sintered metal fiber felts. For illustration, the expected frequency is selected as 500 Hz for the case of sole-frequency optimization, while the expected frequency range is set to be 500–1000 Hz for the case of frequency-range optimization.

Figure 6(a) compares the sound absorption coefficients of non-optimized (uniform and linearly gradient) metal fiber samples with that of sole frequency optimized sample. In particular, results for the case of linear porosity distribution are included to highlight the effect of porosity distribution optimization on sound absorption. Relevant physical parameters employed for the comparison are listed in Table 2. Corresponding results for frequency-range optimization are presented in Figure 6(b). It is seen from Figure 6(a) and (b) that, for both sole frequency and frequency-range optimization, the sound absorption performance of sintered metal fiber felt is greatly enhanced by optimizing the distribution of its porosity.

To reveal the details of porosity distribution, the porosity of each layer is displayed in Figure 7(a) and (b), for sole frequency and frequency-range optimized samples, respectively. Here, Layer 1 in the multilayer sample (Table 2) is the layer placed immediately next to the rigid wall (Figure 3). It is seen from Figure 7 that, even though the optimized samples for sole frequency and frequency range are composed of different numbers of layers, the porosities of both samples first increase then decrease with increasing distance from the incident plane. For instance, in the frequency-range optimized sample (Figure 7(b)), the first layer (Layer 6) has a porosity lower than that of the last layer (Layer 1) while the third layer (Layer 4) has the highest porosity.

### 4.2 Optimized fiber diameter distribution

To optimize the distribution of fiber diameter, the target multilayer sample has a fixed thickness of 10 mm and a fixed porosity of 90%. Similar to the case of porosity optimization, 500 and 500–1000 Hz are selected for sole frequency and frequency-range optimization, respectively.

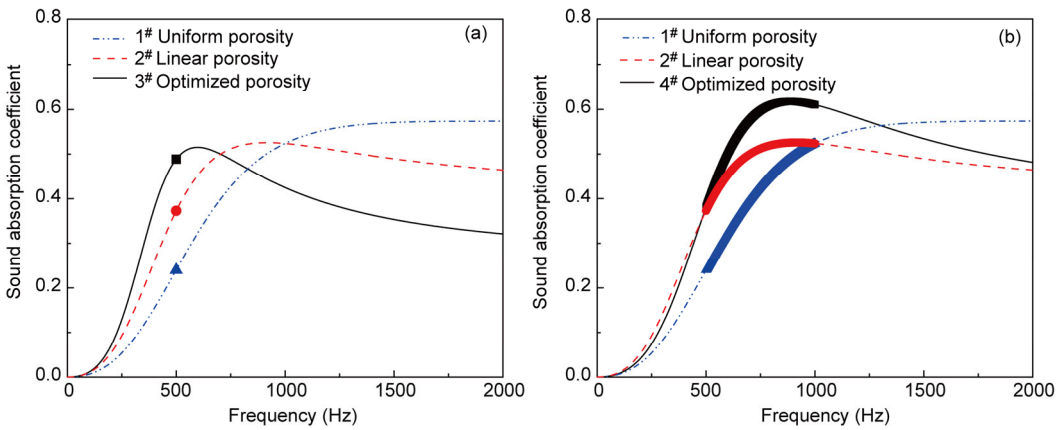


**Figure 6** (Color online) Comparison of sound absorption coefficients among sintered metal fiber samples with optimized, uniform and linearly gradient porosity distributions: (a) sole frequency (500 Hz) optimization and (b) frequency-range (500–1000 Hz) optimization.

**Table 2** Physical parameters of porosity optimized and non-optimized sintered metal fiber samples

| Sample number | Layer arrangement | Porosity (%) | Fiber diameter (μm) | Thickness of layer (mm) |
|---|---|---|---|---|
| 1# | Single layer | 78.3 | 20 | 10.0 |
| 2# | 1st | 95 | 20 | 2.57 |
| | 2nd | 85 | 20 | 5.0 |
| | 3rd | 75 | 20 | 1.82 |
| | 4th | 65 | 20 | 0.61 |
| 3# | 1st | 74 | 20 | 2.57 |
| | 2nd | 87.2 | 20 | 5.0 |
| | 3rd | 91.9 | 20 | 1.82 |
| | 4th | 60 | 20 | 0.61 |
| 4# | 1st | 78.7 | 20 | 2.39 |
| | 2nd | 88.1 | 20 | 2.83 |
| | 3rd | 91.3 | 20 | 2.83 |
| | 4th | 94.3 | 20 | 1.02 |
| | 5th | 92.8 | 20 | 0.5 |
| | 6th | 60.4 | 20 | 0.43 |

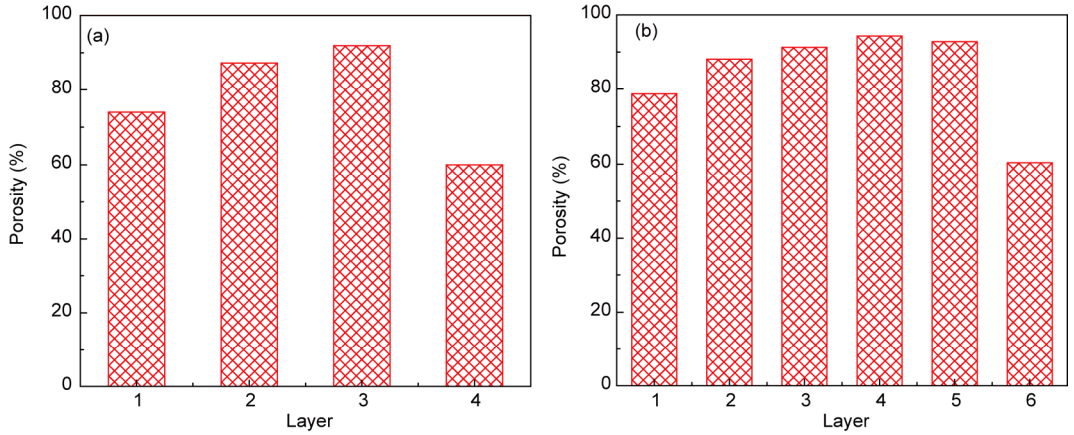


**Figure 7** (Color online) Porosity distribution in porosity optimized metal fiber sample: (a) sole frequency optimization (Sample 3# in Figure 6(a)) and (b) frequency-range optimization (Sample 4# in Figure 6(b)).

As previously discussed concerning Figure 5(b), the sound absorption coefficient of sintered metal fiber felt decreases with increasing fiber diameter at low frequencies. Therefore, for sole frequency (500 Hz) optimization, the optimized fiber diameter should be the lower bound 6.5 μm. For frequency-range optimization, the sound absorption coefficients of optimized, uniform and linearly gradient sintered metal fiber samples are compared in Figure 8. Corresponding physical parameters of these samples are listed in Table 3. For the optimized multilayer sample, Figure 9 presents the distribution of fiber diameter across its thickness (10 mm).

The results of Figure 8 indicate that, within the frequency range considered, the optimized metal fiber sample absorbs sound better than other samples. Further, as shown in Figure 9, the fiber diameter first increases then decreases as the distance from the incident plane is increased.

### 4.3 Optimized porosity and fiber diameter distribution

Consider again a 10 mm thick metal fiber multilayer. The distributions of its porosity and fiber diameter are optimized simultaneously. Figure 10(a) and (b) compares the sound absorption coefficients of sole frequency and frequency range optimized samples with those of non-optimized (uniform and linearly gradient) samples, respectively, while Table 4 compares the physical parameters associated with these samples. It can be seen from Figure 10 that, at the expected frequency (500 Hz) or within the expected frequency range (500–1000 Hz), the sound absorption coeffi-

**Table 3** Physical parameters of metal fiber samples with optimized (frequency range) and non-optimized fiber diameter distributions

| Sample number | Layer | Porosity (%) | Fiber diameter (μm) | Thickness of the layer (mm) |
|---|---|---|---|---|
| 5# | Single layer | 90 | 6.5 | 10.0 |
| 6# | 1st | 90 | 7 | 1.84 |
| | 2nd | 90 | 8 | 4.33 |
| | 3rd | 90 | 9 | 3.83 |
| 7# | 1st | 90 | 6.5 | 1.84 |
| | 2nd | 90 | 11.44 | 4.33 |
| | 3rd | 90 | 6.5 | 3.83 |

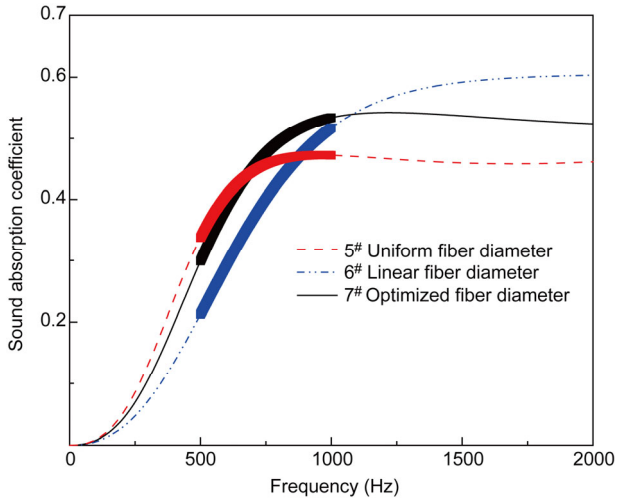


**Figure 8** (Color online) Comparison of sound absorption coefficients among sintered metal fiber samples with uniform, linearly gradient and frequency range (500–1000 Hz) optimized fiber diameter distributions.

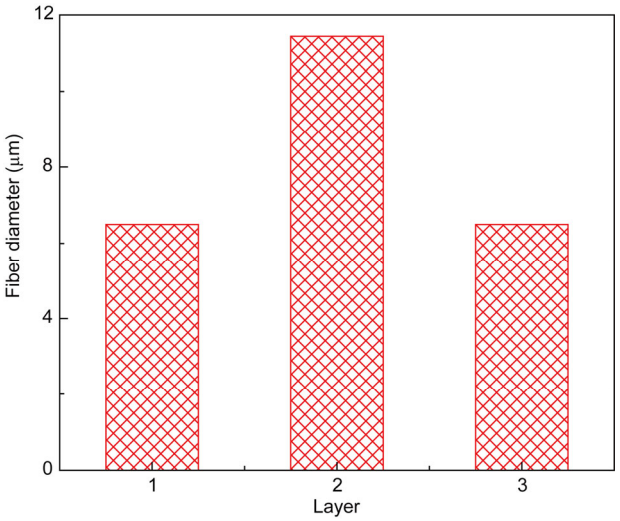


**Figure 9** (Color online) Distribution of fiber diameter in metal fiber sample with frequency-range optimized fiber diameters (Sample 7# in Figure 8).

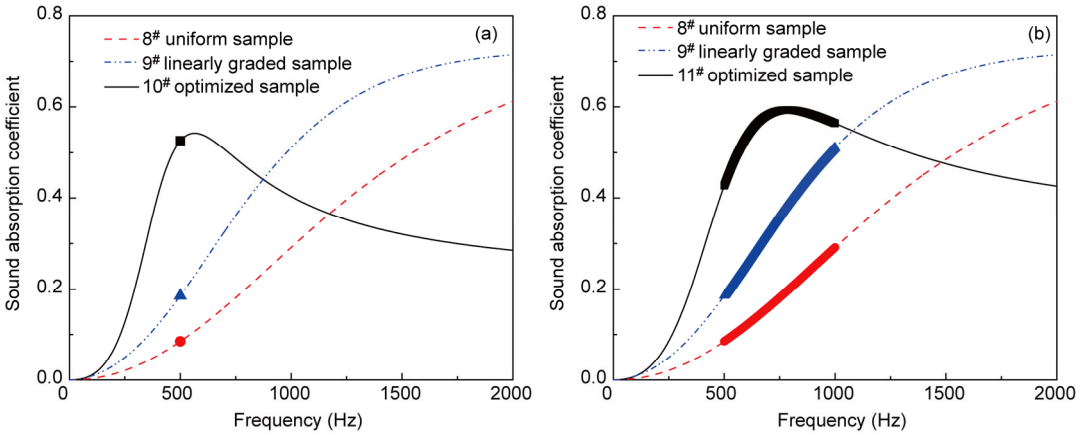


**Figure 10** (Color online) Comparison of sound absorption coefficients among metal fiber samples with optimized, uniform and linearly gradient porosity and fiber diameter distributions: (a) sole-frequency (500 Hz) optimization and (b) frequency-range (500–1000 Hz) optimization.

**Table 4** Physical parameters of porosity and fiber diameter optimized metal fiber samples and non-optimized samples

| Sample number | Layer | Fiber diameter (μm) | Porosity (%) | Thickness of the layer (mm) |
|---|---|---|---|---|
| 8# | Single layer | 49.4 | 74 | 10.0 |
| | 1st | 50 | 95 | 4.4 |
| | 2nd | 40 | 90 | 2.1 |
| 9# | 3rd | 30 | 85 | 1.6 |
| | 4th | 20 | 80 | 1.6 |
| | 5th | 10 | 75 | 0.3 |
| | 1st | 77 | 63 | 4.4 |
| | 2nd | 42 | 80 | 2.1 |
| 10# | 3rd | 48 | 86 | 1.6 |
| | 4th | 68.8 | 79 | 1.6 |
| | 5th | 11 | 61 | 0.3 |
| | 1st | 37 | 76 | 4.0 |
| | 2nd | 37 | 72 | 0.8 |
| 11# | 3rd | 100 | 73 | 0.8 |
| | 4th | 16 | 94 | 4.0 |
| | 5th | 6.52 | 72 | 0.4 |

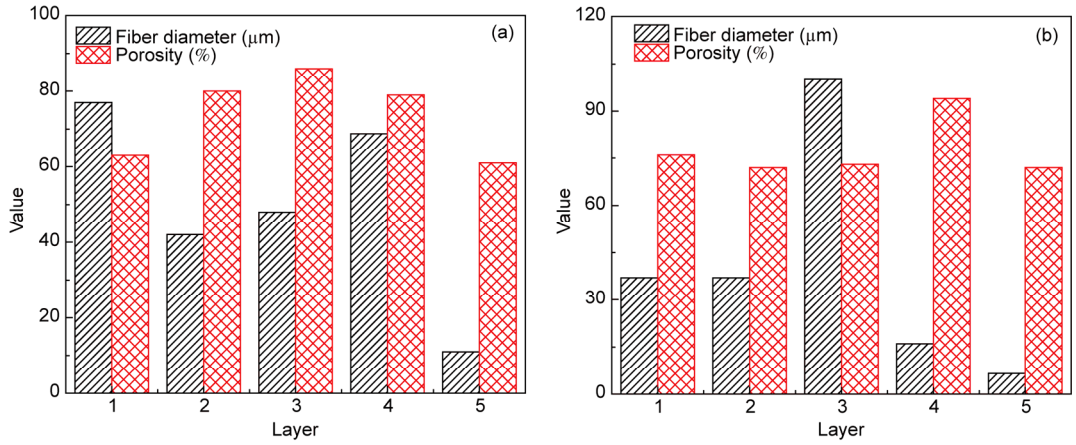


**Figure 11** (Color online) Porosity and fiber diameter distributions in optimized metal fiber samples: (a) sole frequency optimization (Sample 10# in Figure 10(a)) and (b) frequency-range optimization (Sample 11# in Figure 10(b)).

cient of the sample is dramatically improved by optimization, demonstrating again the effectiveness of the present optimization method.

To clearly show the results of optimization, Figures 11(a) and (b) present the distribution of fiber diameter and porosity in each layer of the optimized samples. For sole frequency optimization, as the distance from the incident plane is increased, the porosity first increases then decreases while the fiber diameter first increases then decreases before increasing again. For frequency range optimization, the fiber diameter first increases then decreases with increasing distance from the incident plane, whereas the porosity first increases then decreases before increasing again.

## 5 Conclusions

A theoretical method of sound absorption coefficient optimization is presented for sintered metal fiber felts based upon the dynamic flow resistivity model. The sound absorption coefficients of both uniform and gradient (multi-layer) sintered metal fiber samples are measured. Comparison between theoretical predictions and experimental results confirms the accuracy of the theoretical model in evaluating the sound absorption performance of sintered metal fiber felts. Objective functions and constraint conditions are subsequently set up for porosity, fiber diameter, and simultaneous porosity and fiber diameter optimizations at a sole frequency or within a predefined frequency range. It is demonstrated that sintered metal fiber felts with optimized gradient morphologies exhibit superior sound absorption behavior over non-optimized samples at relatively low frequencies.

*This work was supported by the National Natural Science Foundation of China (Grant No. 51528501), and the Fundamental Research Funds for Central Universities (Grant No. 2014qngz12). Xin is supported by China Scholarship Council as a visiting scholar to Harvard University.*

1 Sun F, Chen H, Wu J, et al. Sound absorbing characteristics of fibrous metal materials at high temperatures. Appl Acoust, 2010, 71: 221–235
2 Chang B, Wang X, Peng F, et al. Prediction on the sound absorption performance of fibrous porous metals at high sound pressure levels. Tech Acoust, 2009, 28: 450–453
3 Wu J, Hu Z, Zhou H. Sound absorbing property of porous metal materials with high temperature and high sound pressure by turbulence analogy. J Appl Phys, 2013, 113: 194905
4 Zhang B, Chen T, Feng K, et al. Sound absorption properties of sintered fibrous metals under high temperature conditions. J Xi'an Jiaotong Univ, 2008, 42: 1327–1331
5 Meng H, Ao Q, Tang H, et al. Dynamic flow resistivity based model for sound absorption of multi-layer sintered fibrous metals. Sci China Tech Sci, 2014, 57: 2096–2105
6 Delany M E, Bazley E N. Acoustical properties of fibrous absorbent materials. Appl Acoust, 1970, 3: 105–116
7 Miki Y. Acoustical properties of porous Materials-Modifications of Delany-Bazley models. J Acoust Soc Jap (E), 1990, 11: 19–24
8 Komatsu T. Improvement of the Delany-Bazley and Miki models for fibrous sound-absorbing materials. Acoust Sci Tech, 2008, 29: 121–129
9 Allard J F, Champoux Y. New empirical equations for sound propagation in rigid frame fibrous materials. J Acoust Soc Am, 1992, 91: 3346–3353
10 Attenborough K. Acoustical characteristics of rigid fibrous absorbents and granular materials. J Acoust Soc Am, 1983, 73: 785–799
11 Lambert R F, Tesar J S. Acoustic structure and propagation in highly porous, layered, fibrous materials. J Acoust Soc Am, 1984, 76: 1231–1237
12 Allard J F, Atalla N. Propagation of Sound in Porous Media: Modelling Sound Absorbing Materials 2e. Chichester: Wiley, 2009. 73–90
13 Zhang B, Chen T. Calculation of sound absorption characteristics of porous sintered fiber metal. Appl Acoust, 2009, 70: 337–346
14 Shravage P, Bonfiglio P, Pompoli F. Hybrid Inversion technique for predicting geometrical parameters of porous materials. J Acoust Soc Am, 2008, 123: 3284
15 Atalla Y, Panneton R. Inverse acoustical characterization of open cell porous media using impedance tube measurements. Can Acoust, 2005, 33: 11–24
16 Doutres O, Salissou Y, Atalla N, et al. Evaluation of the acoustic and non-acoustic properties of sound absorbing materials using a three-microphone impedance tube. Appl Acoust, 2010, 71: 506–509
17 Zielinski T. Inverse identification and microscopic estimation of parameters for models of sound absorption in porous ceramics. In: Proceedings of International Conference on Noise and Vibration Engi-

neering (ISMA2012)/International Conference on Uncertainty in Structural Dynamics (USD2012), Leuven, 2012. 95–108
18 Bonfiglio P, Pompoli F. Inversion problems for determining physical parameters of porous materials: Overview and comparison between different methods. Acta Acust Unit Acust, 2013, 99: 341–351
19 Liu S, Chen W, Zhang Y. Design optimization of porous fibrous material for maximizing absorption of sounds under set frequency bands. Appl Acoust, 2014, 76: 319–328
20 Chen W, Liu S, Tong L, et al. Design of multi-layered porous fibrous metals for optimal sound absorption in the low frequency range. Theor Appl Mech Lett, 2016, 6: 42–48
21 Tarnow V. Compressibility of air in fibrous materials. J Acoust Soc Am, 1996, 99: 3010–3017
22 Tarnow V. Calculation of the dynamic air flow resistivity of fiber materials. J Acoust Soc Am, 1997, 102: 1680–1688
23 Dupère I D, Dowling A P, Lu T J. The absorption of sound in cellular foams. In: ASME International Mechanical Energineering Congress, Anaheim, IMECE2004-60618, 2004
24 Dupère I D, Lu T J, Dowling A P. Optimization of cell structures of cellular materials for acoustic applications. In: Proc 12th International Congress on Sound and Vibration (ICSV12), Lisbon, 2005
25 Kirby R, Cummings A. Prediction of the bulk acoustic properties of fibrous materials at low frequencies. Appl Acoust, 1999, 56: 101–125
26 Meng H, Xin F X, Lu T J. Sound absorption optimization of graded semi-open cellular metals by adopting the genetic algorithm method. J Vib Acoust, 2014, 136: 061007